IEEE Access
Multidisciplinary | Rapid Review | Open Access Journal

Received January 10, 2020, accepted January 23, 2020, date of publication January 28, 2020, date of current version February 5, 2020.

Digital Object Identifier 10.1109/ACCESS.2020.2969964

A Metasurface-Based Low-Profile Wideband Circularly Polarized Patch Antenna for 5G Millimeter-Wave Systems

NIAMAT HUSSAIN, MIN-JOO JEONG, ANEES ABBAS, TAE-JUN KIM, AND NAM KIM
Department of Computer and Communication Engineering, Chungbuk National University, Cheongju 28644, South Korea

Corresponding author: Nam Kim (namkim@chungbuk.ac.kr)

This work was supported by the ICT Research and Development Program of MSIT/IITP, South Korea (A Study on Public Health and Safety in a Complex EMF Environment) under Grant 2019-0-00102.

ABSTRACT This paper presents the design and realization of a metasurface-based low-profile wideband Circularly Polarized (CP) patch antenna with high performance for Fifth-generation (5G) communication systems. The antenna consists of a modified patch, sandwiched between an array of 4×4 symmetrical square ring Metasurface (MTS) and a ground plane. Initially, the intrinsic narrow bandwidth of the conventional patch antenna is increased using a diagonal rectangular slot. For further performance enhancement, the additional resonances and CP radiations are achieved for wideband operation in terms of impedance and Axial Ratio (AR) by effective excitation of surface waves propagating along the MTS. The stacking of MTS on the modified patch without any air gap resulted in an overall compact size of $1.1\lambda_0 \times 1.1\lambda_0 \times 0.093\lambda_0$. Simulated and measured results show that the MTS-based antenna offers a wide impedance bandwidth ranging from 24 – 34.1 GHz (34.7%) for $|S_{11}| < -10$ with a maximum gain of 11 dBic and a 3-dB AR bandwidth of 24.1 – 29.5 GHz (20.1 %). Moreover, the proposed antenna has a smooth gain response with a small variation in its gain (9.5 – 11 dBic) and a stable left-hand CP radiation in the desired frequency range. The operating bandwidth of this antenna is covering the proposed entire global millimeter-wave spectrum (24.2 – 29.5 GHz) for 5G communication systems.

INDEX TERMS Metasurface-based antenna, circular polarization, 5G technology, millimeter-wave.

I. INTRODUCTION

The congestion, limited bandwidth and restricted channel capacity of the current wireless system have pushed researchers and engineers to utilize an unused Millimeter-Wave (MMW) spectrum in Fifth-generation (5G) of wireless communication systems [1]. The upcoming 5G communication systems are not only promised to meet the exponentially increasing demands of high data rates, reliability, and low power consumption for the billions of connected devices around us, but also capable to unlock the full capabilities of the emerging technologies such as smart cities, virtual reality, and autonomous cars [2], [3]. Researchers from all over the globe are working towards the development and the standardization of the 5G communication systems. Two kinds of frequency bands are expected to be used for 5G; the currently existing sub-6-GHz frequency band for wide-area coverage and a new MMW frequency band for very high data rates with low-latency. Most of the countries (USA, UK, Canada, European Union, China, Japan, Korea, etc) have chosen MMW frequency bands within the frequency range from 24.2 – 29.5 GHz for their future 5G communications [4]. The detailed global snapshot of 5G spectrum is given in Fig. 1.

Besides operating frequency, Circular Polarization (CP) is one of the most promising features in the design of the antenna, as it shows greater immunity to interferences, multipath distortions, and fading robustness with better mobility and flexible orientation for the antennas. This is the reason the CP is a popular choice for wireless and satellite communications, particularly in randomly oriented RFID tags, wireless sensors, and device-to-device communication systems. The microstrip patch antennas are preferred in the design of CP antennas due to their planar structure, low-cost, planar structure, and easy integration with other electronic

The associate editor coordinating the review of this manuscript and approving it for publication was Weiren Zhu.

	<1 GHz	3GHz	4GHz	5 GHz	24–28 GHz	37–40 GHz	64–71GHz
	600 MHz	3.5GHz		5.9–7.1GHz	27.5–28.35GHz	37–37.6GHz	64–71GHz
	600 MHz	3.5GHz		5.9–7.1GHz	27.5–28.35GHz	37.6–40GHz	64–71GHz
	700 MHz	3.4–3.8GHz		5.9–6.4GHz	24.5–27.5GHz	37–37.6GHz	
		3.4–3.8GHz			26, 28GHz	37–40GHz	
		3.4–3.7GHz			26, 28GHz		
		3.46–3.8GHz			26GHz		
		3.6–3.8GHz					
		3.3–3.6GHz			24.5–27.5GHz	37.5–42.5GHz	
		3.4–3.7GHz	4.8–5GHz		26.5–29.5GHz		
		3.6–4.2GHz			27.5–29.5GHz		
		3.4–3.7GHz	4.4–4.9GHz		28 GHz	39GHz	

FIGURE 1. The global snapshot of 5G spectrum.

circuits. However, these antennas suffer from the disadvantages of low bandwidth and gain. Many studies have been carried out to overcome the intrinsic low gain and narrow Axial Ratio (AR) of the single-fed CP patch antennas. The use of thick superstrate above the radiator with an air gap (Fabry-Perot cavity antennas) increases the gain and the AR bandwidth significantly [5]–[8], however, these designs possess poor mechanical properties due to the presence of air gap and have high-profiles. Although, the antennas with multiple stacked substrates without air gap have wideband CP radiations [9], [10] but have the drawbacks of complex design and non-planar structures.

On the other hand, metasurfaces which are the two-dimensional equivalent of the metamaterials are combined with radiators to achieve wideband AR and gain enhancement, while keeping the low-profile of the antennas [11]–[29]. Essentially the metasurface (MTS) is placed either above [11]–[16] or below [17]–[21] the radiator with an air gap. These configurations have design complexities, high-profiles, and poor mechanical properties because of the air gap. Alternatively, the MTS is directly stacked on the radiator without any air gap to design low-profile wideband CP antennas [22]–[29]. However, these designs are at microwave frequencies. It is evident from the literature review that antenna design at MMW frequencies is quite challenging due to the very small physical size of the antenna. This has somehow restricted the design of CP MTS antennas at high frequencies. Although, a few MTS antennas have been designed at MMWs [30]–[34], have linear polarization. To the best of the authors' knowledge, none of the reported circularly polarized planar antennas [35]–[39] cover the entire designated 5G MMW band (24.1 – 29.5 GHz). A light-weight, low-profile and low-cost antenna having mass-production suitability as well as having a desirable bandwidth and gain is the need of the time.

On the basis of the above considerations, a planar MTS-based wideband circularly polarized patch antenna for 5G communication systems is proposed. The whole idea of this work is to design a low-profile, CP antenna with a decent gain to covers the entire allocated MMW 5G spectrum. Initially, a rectangular slot is etched on the truncated corner patch antenna to overcome the narrowband characteristics of the conventional CP patch antenna. The antenna performance

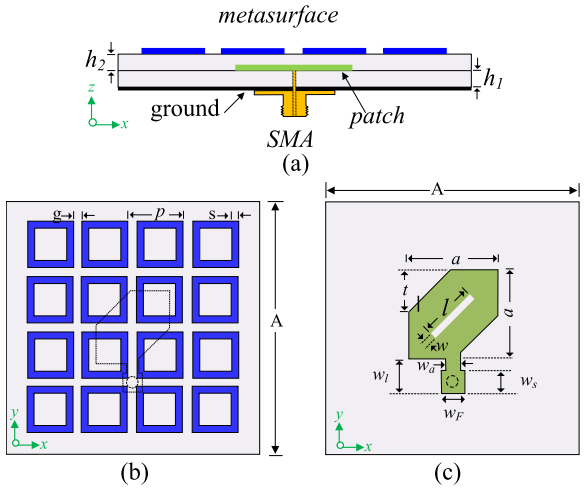

FIGURE 2. The geometry of the proposed metasurface antenna: (a) Side view of the antenna, (b) top view of the metasurface, and (c) top view of the patch.

is further improved in terms of gain, and especially the impedance and AR bandwidths by stacking a well-designed rectangular ring MTS on the patch antenna without any air gap. The operating bandwidth of the proposed design covers the MMW 5G band spectrum (24.1 – 29.5 GHz) with a moderate gain of 11 dBic and has low-profile, mass-production suitability.

II. ANTENNA GEOMETRY

The geometry and schematics of the proposed antenna are shown in Fig. 2. The antenna is consisting of a modified square patch, sandwiched between a MTS and a grounded substrate. The square patch has dimensions of $a \times a$ whose one set of corners are truncated for CP radiations. A rectangular diagonal slot with a length and width of l and w, respectively, is inserted into the patch to enhance the intrinsic narrow operating bandwidth of the single-fed CP patch antenna. The MTS consists of an array of 4×4 symmetrical square rings which has a periodicity of P, while the gap between the adjacent unit cells is defined as g. The MTS and the radiator are printed on two identical high frequency substrate layers of Rogers 5880 ($\varepsilon_r = 2.2$, $tan\delta = 0.0009$, $h = 0.51$ mm). The MTS layer is directly stacked above the patch without any air gap to achieve the low-profile of the antenna. The antenna has an overall size of only $12 \times 12 \times 1.02$ mm^3 which corresponds to $1.1\lambda_0 \times 1.1\lambda_0 \times 0.093\lambda_0$, where λ_0 is free-space wavelength at 27.5 GHz. The parameters for the optimum performance of the antenna are as under: $A = 12$, $h_1 = 0.51$, $h_2 = 0.51$, 1 $p = 2.3$, $g = 0.5$, $s = 0.3$, $w = 0.2$, $l = 1$, $w_F = 0.8$, $L_F = 1$, $w_a = 0.6$, $w_s = 0.8$, $t = 0.5$, and $a = 3.2$ (unit = mm).

III. ANTENNA DESIGN PROCEDURE

This section explains the detailed design procedure of the proposed MTS-based wideband CP antenna. For ease of understanding, it is divided into the following sub-sections.

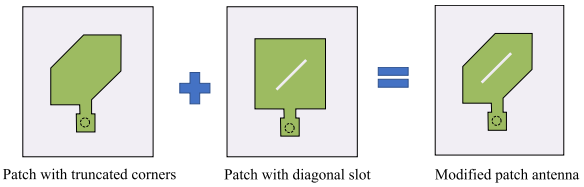

FIGURE 3. The design evolution of the modified CP patch antenna.

A. DESIGN OF THE MODIFIED PATCH ANTENNA

The design of the proposed antenna starts from the simulation of a simple square patch antenna chosen to operate at TM_{01} mode. The size of the patch at the central resonating frequency (f_{res}) is calculated as follows:

$$a = \frac{c}{2f_{res}\sqrt{\varepsilon_{eff}}} \tag{1}$$

$$\varepsilon_{effective} = \frac{\varepsilon_r + 1}{2} \tag{2}$$

where, c is the speed of light, ε_r is the relative dielectric constant and $\varepsilon_{effective}$ is the effective dielectric constant of the substrate. The antenna is fed by the 50-ΩK-connector through a microstrip line with dimensions of $w_a \times w_l$. For proper connection of the connector to the feedline, an additional pad ($w_s \times w_F$) is defined at the end of the microstrip line. As the antenna size is very small, severe effects on radiation can be seen due to the connector, if not fed properly. The patch is fed from the bottom by extending the inner pin of the connector pad to minimize connector effects.

As square patch antennas have linear polarization, perturbation techniques are employed to achieve CP radiation. The most common and convenient way is by truncating a set of patch corners or inserting a rectangular diagonal slot into the patch [40]. Tuning the corner truncation and slot dimensions is used to adjust the magnitudes and phases of the two orthogonal modes and thus, CP radiation is achieved. Several techniques including, inserting slots of different shapes (U, cross, circular ring, and square shaped-slots) have been employed to improve the narrowband characteristics of the single-fed CP patch antennas [41]–[44]. In this design, we combined both traditional techniques (truncation of patch corners and insertion of the diagonal slot in the patch) of achieving CP by inserting a rectangular diagonal slot into the truncated patch antenna. The design evolution of the modified CP patch antenna is shown in Fig. 3. The impedance and AR bandwidths of the antenna are increased by overlapping the individual resonances of the patch and slot as shown in Fig. 4(a). The truncated corner patch antenna without rectangular slot has −10 dB impedance bandwidth from 26.9 to 28.4 GHz, however, this antenna with rectangular diagonal slot gave a wider impedance bandwidth from 26 to 28.2 GHz with an additional resonance at lower frequencies. The slot provides a longer path for current to flow, thus the resonance corresponding to the diagonal slot is observed at lower frequencies. A similar phenomenon can be seen for the AR response as depicted in Fig. 4(b). The antenna without slot

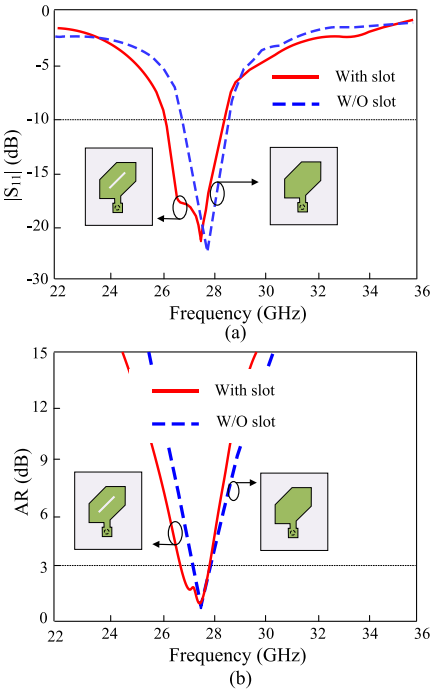

FIGURE 4. Characteristics of the modified patch antenna with and without diagonal slot: (a) $|S_{11}|$, and (b) AR.

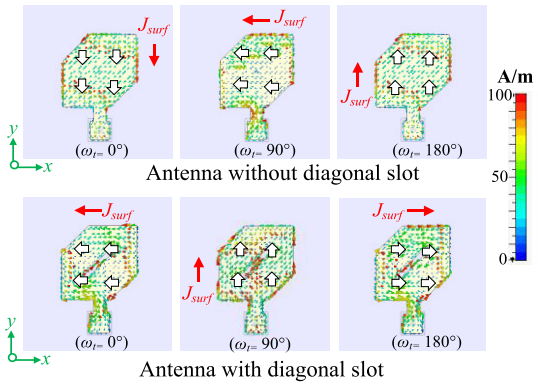

FIGURE 5. Surface current distributions of the patch antenna with and without diagonal slot at their resonance frequencies.

shows a 3-dB AR bandwidth ranging from 27.2 – 27.9 GHz which increased to 26.7 – 27.85 GHz with two minimum AR points for the antenna with the rectangular slot. We plotted the surface current (J_{surf}) distributions on the patch antenna with and without rectangular slot at their resonance frequencies of 27.5 GHz and 27.2 GHz, respectively (Figure 5). The J_{surf} rotates in the clockwise direction for different phase values ($\omega_t = 0°$, $\omega_t = 90°$, and $\omega_t = 180°$), which demonstrates the CP radiations of the antennas.

B. DESIGN OF METASURFACE-BASED WIDEBAND CP PATCH ANTENNA

Metasurfaces have been widely used in the design of the patch antennas to increase both impedance and AR bandwidths. As discussed earlier, the small physical size of the antenna at

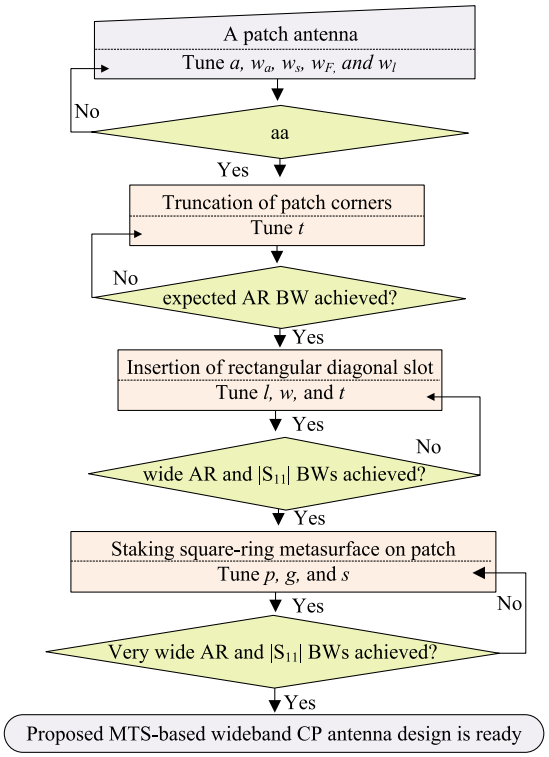

FIGURE 6. The design procedure and optimization of the proposed metasurface-based wideband CP antenna.

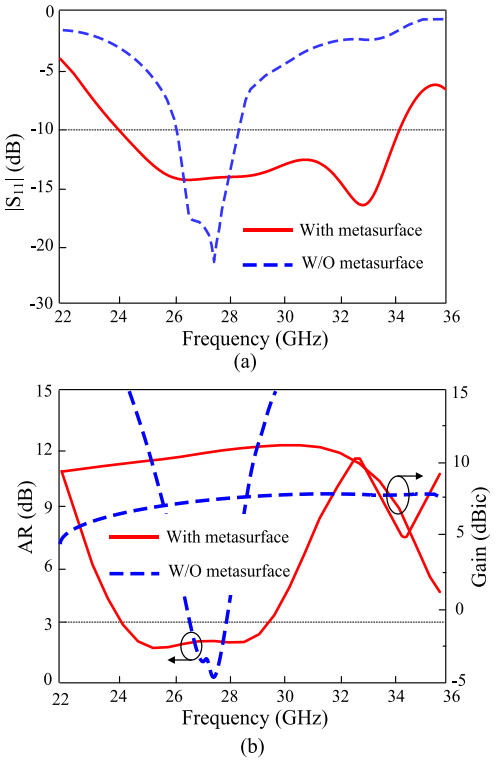

FIGURE 7. Characteristics of the antenna with and without metasurface: (a) $|S_{11}|$, (b) AR, and broadside gain.

MMW frequencies has restricted the design of MTS antennas at high frequencies. For example, the antenna size in is smaller than the connector size, which may deteriorate the radiation patterns, when not fed properly. Keeping all such design constraints in mind, the MTS is integrated with the antenna. The proposed metasurface-based wideband CP patch antenna designed by directly stacking a periodic lattice of 4 × 4 square rings MTS layer on the modified patch antenna depicted previously in Fig 2. The directly stacking of the MTS layer on the patch without any air gap enabled a very low-profile of the antenna (overall thickness=1.02 mm), makes it suitable for compact smart 5G devices. The detailed insight about the design procedure and optimization process of the antenna are summarized in the flowchart, shown in Fig. 6. It can be seen from the flowchart that how the antenna is designed and what are the important design parameters that play a role in the optimization of impedance and AR bandwidths of the antenna. To demonstrate the wideband characteristics of the metasurface-based CP path antenna, its $|S_{11}|$ and radiation characteristics are studied.

Figure 7 shows the simulated $|S_{11}|$, AR, and broadside gain of the proposed antenna with and without metasurface. The additional resonances and CP radiations are achieved for wideband operation in terms of $|S_{11}|$ and AR by effective excitation of surface waves propagating along the MTS [45]. The $|S_{11}|$ bandwidth of the antenna with MTS is increased by almost 400 %, while AR bandwidth is improved up to 500 % compared to the antenna without metasurface. The use of the square ring MTS did not only improve bandwidth but also the gain of the antenna. The gain of the patch is noted to be 7.5 dBic, which increased to 11 dBic for the patch antenna with MTS. In addition, the performance of the proposed MTS antenna in terms of $|S_{11}|$, AR, and maximum broadside gain is compared with its parent designs, that is, truncated corner square patch antenna and truncated corner square patch antenna with a rectangular slot, are summarized in Table 1.

TABLE 1. Performance summary for different antenna configurations.

Antennas	-10 dB $\|S_{11}\|$ BW	3-dB AR BW	Max. Gain
Antenna W/O diagonal slot	5.4 % (26.9 – 28.4 GHz)	2.54 % (27.2–27.9 GHz)	7.5 dBic
Antenna with diagonal slot	8.12 % (26.0 – 28.2 GHz)	4.2% (26.7–27.85 GHz)	7.5 dBic
Proposed MTS antenna	34.7% (24 – 34.1 GHz)	20.1 % (24.1–29.5 GHz)	11 dBic

IV. RADIATION MECHANISM OF THE ANTENNA

The performance, especially the operating bandwidth of the CP patch antennas are improved by utilizing periodic structures as MTS. It generates additional resonances produced by surface waves propagating on the MTS of finite size. These additional resonances are utilized effectively to increase $|S_{11}|$

and AR bandwidths. This technique has already been thoroughly investigated in [17], [18], [45]. The operating central frequency can be simply predicted by:

$$\beta_{sw} = \frac{m\pi}{L_{MTS}} \quad m = 1, 2, 3, \ldots \tag{3}$$

$$L_{MTS} = P \times N_{(x,y)} \tag{4}$$

Here, β_{sw} is the propagation constant of the surface wave at resonance frequency, L_{MTS} is the length of the MTS array, while P is the periodicity and $N_{(x,y)}$ is the number of unit cells in x- and y- direction [18]. The propagation constant of transverse electric (TE) and transverse magnetic (TM) waves can be calculated as.

$$\beta_{TE} = \frac{\omega}{c}\sqrt{1 - \frac{(Z_{MTS})^2}{(Z_0)^2}} \tag{5}$$

$$\beta_{TM} = \frac{\omega}{c}\sqrt{1 - \frac{(Z_0)^2}{(Z_{MTS})^2}} \tag{6}$$

where ω is the angular frequency, c is the speed of light, and Z_{MTS} is the surface impedance of MTS while Z_0 is the free space impedance.

The dispersion diagram of the MTS at first two eigenmodes, TM and TE, is plotted in Fig. 7. It shows that when the phase shift of the unit cell is 90°, the intersection between the dispersion curves and the vertical line representing the solution of (3) indicates the resonant frequency of the MTS. The TE and TM surface waves are predicted to resonate at around 27 GHz for a metasurface configuration of $N_{(x,y)} = 4\times4$ unit-cells. Here, $m = 2$ is considered, since the surface waves are likely to excite as slow-wave propagation supported around the patch resonance.

The reflection phase characteristics of the MTS unit cell show that the periodic square-ring MTS behaves as High Impedance Surface (HIS) supporting in-phase reflections for an incident wave over a certain bandwidth (Fig. 8(c)). In practice, the reflection phase of HIS varies continuously from 180° to −180° versus frequency and takes zero value just at one frequency. This fact is fundamental in the design of low-profile antennas, as the parallel image currents appear in-phase, and so, efficient radiation for antennas placed close to the radiator is possible. The resonance frequency for the 0° reflection phase for the square ring is 27 GHz. The ± 90° reflection phase bandwidth is from 24 GHz to 34 GHz, suggesting the broadband operating frequency of the metasurface.

Furthermore, the frequency characteristics of the square ring MTS can also be predicted using the equivalent circuit diagram, which can be represented using a resonant circuit comprises of capacitance and inductance. As depicted in Fig. 9, the square ring MTS can be detached into two vertical and horizontal stripes. The two neighboring vertical strips form a one equivalent horizontal strip with a width *'2s'* acts as the inductive part, while the two adjacent horizontal stripes are approximated as the capacitive part. Hence, the MTS is approximated as a simple resonant LC circuit shunted

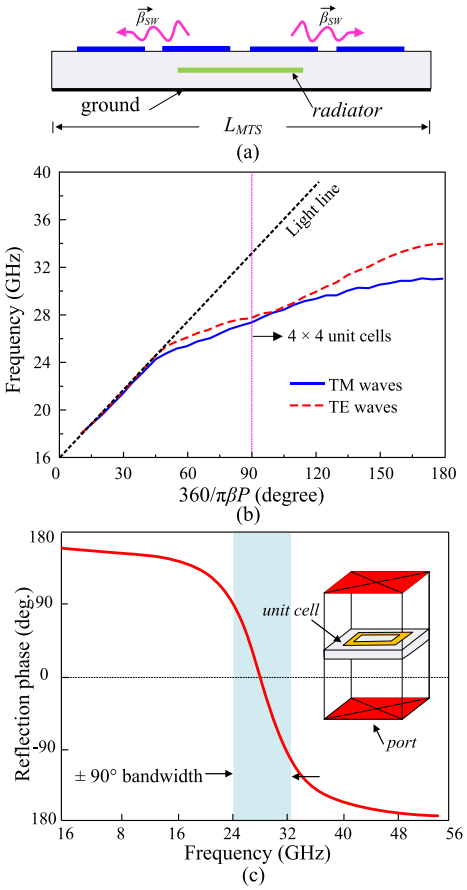

FIGURE 8. Radiation mechanism of the proposed antenna: (a) Surface wave propagation, (b) dispersion diagram, and (c) reflection phase characteristics of the square ring metasurface.

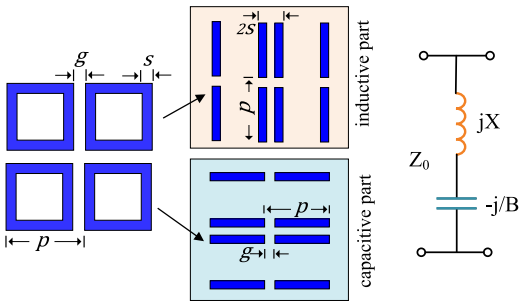

FIGURE 9. Detailed equivalent circuit diagram of the proposed square ring metasurface.

across a transmission line having a free-space characteristic impedance of Z_0. The normalized inductive reactance X and capacitive susceptance B of the square ring MTS can be written as:

$$X = \frac{X_L}{Z_0} = \omega\frac{L_{MTS}}{Z_0} = \frac{p}{(p+g)}F\,(p, 2s, \lambda) \tag{7}$$

$$B = \frac{B_C}{Y_0} = \omega\frac{C_{MTS}\varepsilon_{eff}}{Y_0} = \frac{4p\varepsilon_{eff}}{(p+g)}F\,(p, g, \lambda) \tag{8}$$

Here, Z_0 is the free space impedance which is equal to $Z_0 = 1/Y_0$, ω represents angular frequency, L_{MTS} and C_{MTS}

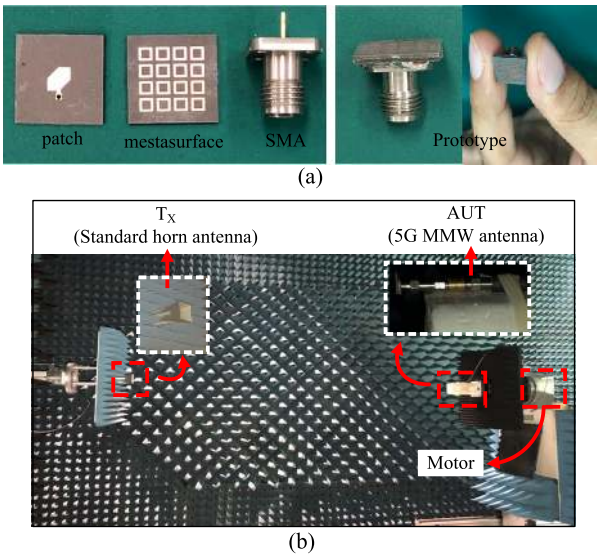

FIGURE 10. Photographs of the (a) fabricated antenna and its parts of the assembly, and (b) far-field measurement setup.

are denoting free-standing inductance and capacitance of the MTS, respectively. The inductive reactance and capacitive susceptance are X_L and B_C respectively, while ε_{eff} is the effective permittivity. The detailed explanation of the equivalent circuit model of such metasurfaces is well described in [46].

V. RESULTS AND DISCUSSION

A prototype of the propose metasurface-based wideband CP antenna is fabricated through photolithography to validate the design concept. The photographs of the fabricated antenna and its part of the assembly, and the far-field measurement setup are illustrated in Fig. 10. A 50-Ω 2.92mm K-connector is connected carefully with the patch, while the MTS layer is directly stacked on a patch antenna with the help of an adhesive liquid. The far-field measurements are done at the anechoic chamber. A well-calibrated standard gain horn antenna (SGH-series) is used as a transmitting antenna (T_X), while the proposed antenna is measured as a receiving antenna (R_X). Amplifiers were used to supply stable power reception. The antenna under test is rotated to get measure the radiation intensity at different orientations. In general, a good agreement between the simulated and measured results are observed.

A. S-PARAMETER

Figure 11 shows the simulated and the measured S-parameter ($|S_{11}|$) of the antenna. The $|S_{11}|$ is measured using a network analyzer (Rohde and Schwarz ZVA 40) in an open-air condition. It can be seen that the antenna has a good impedance matching ($|S_{11}| < -10$ dB) in a broadband frequency starting from 24 to 34.1 GHz, equivalent to a fractional bandwidth of 34.7 % with respect to the central frequency.

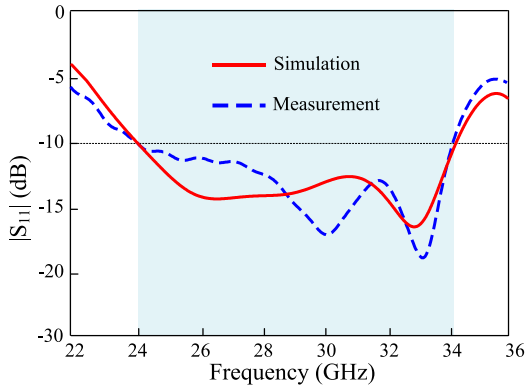

FIGURE 11. S-parameter $|S_{11}|$ of the proposed metasurface antenna.

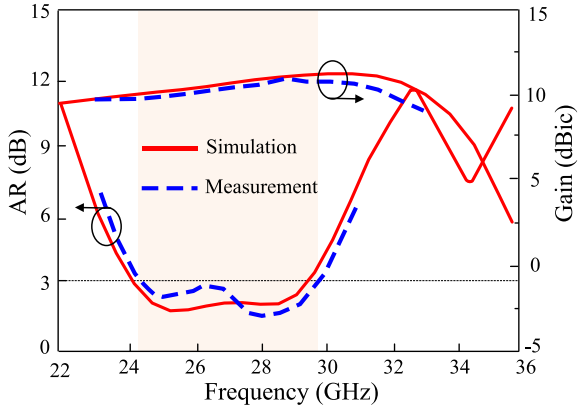

FIGURE 12. Axial ratio and broadside gain of the proposed metasurface antenna.

B. AR AND BROADSIDE GAIN

The antenna radiation properties in terms of AR and broadside gain are illustrated in Fig. 12. The measured 3-dB AR bandwidth is 20.1 %, ranging from 24.1 to 29.5 GHz, and this band is fully overlapped by the impedance bandwidth. A little variation between measured and simulated AR curves are due to miss alignment of the MTS layer on the patch and the fabrication imperfections. In addition, the broadside gain varies from 9.5 to 11 dBic within the operating bandwidth (24.1–29.5 GHz). The measured gain values are little lower than the simulated one, it may be due to the increased substrate/insertion losses at high frequencies.

C. RADIATION PATTERNS

The radiation patterns in both principal planes (xoz and yoz-plane) at 25, 28, and 31 GHz are plotted in Fig. 13. The antenna has stable and symmetrical radiation patterns with left-hand CP (LHCP) radiation. It can be seen that the right-hand CP (RHCP) is very small compared to the LHCP radiation across the operating bandwidth. At the broadside direction ($\theta = 0°$), the LHCP level is more than 13 dB compared to the RHCP level. To get a better insight of the polarization, the electric-field (E-field) of the antenna

TABLE 2. Performance comparison of the proposed antenna with state-of-the-art works.

Refs.	Antenna type	Antenna size (λ_0^3)	f_c (GHz)	LP/ CP	-10 dB $\|S_{11}\|$ BW (%)	3dB AR BW (%)	Max. Gain	Printed layers	Air gap	Satisfy 5G MMW band (24.2–29.5 GHz)
[8]	Fabry-Perot	2.50×2.50×1.44	30	CP	8.2	2.98	15 dBic	3	Yes	Partially satisfied
[9]	Stacked patch	0.63×0.63×0.14	5	CP	41	16.8	7.4 dBic	5	No	Not satisfied
[14]	Stacked patch	0.81×0.81×0.09	6	CP	30	20.3	8.6 dBic	3	Yes	Not satisfied
[16]	MTS antenna	1.0×1.0×0.35	30	CP	19	6	8 dBic	3	Yes	Partially satisfied
[17]	MTS antenna	0.72×0.72×0.6	6	CP	36.2	32.2	7.0 dBic	3	Yes	Not satisfied
[28]	MTS antenna	1.4×1.4×0.072	5.6	CP	38.8	14.3	8.5 dBic	2	No	Not satisfied
[29]	MTS antenna	1.05×0.97×0.07	4.8	CP	46.52	28.9	6.8 dBic	2	No	Not satisfied
[33]	MTS antenna	0.92×0.92×0.20	26.5	LP	4.8	-	7.9 dBi	2	No	Partially satisfied
[34]	EBG antenna	3.13×2.67×0.03	28	LP	40	-	7.9 dBi	2	No	Completely satisfied
[35]	H-S antenna	0.18×0.22×0.11	28	CP	2.14	0.47	4.5 dBic	4	No	Partially satisfied
[36]	Cross-dipole	0.19×0.19×0.15	28	CP	8	8	2.2 dBic	1	No	Partially satisfied
[37]	MTM antenna	1.18×0.88×0.27	29.5	CP	22.5	7.4	10 dBic	3	No	Partially satisfied
[38]	EBG antenna	13.7×13.7×0.37	29.5	CP	17.2	10	11.9dBic	2	yes	Partially satisfied
Prop.	**MTS antenna**	**1.10×1.10×0.093**	**27.5**	**CP**	**34.7**	**20.1**	**11 dBic**	**2**	**No**	**Completely satisfied**

BW stands for bandwidth, λ_0 stands for free space wavelength at central frequency (f_c)*, CP/LP stands for linear/circular polarization, EBG stands for electromagnetic bandgap, H-S stands for Huygens source, and MTM stands for metamaterial.*

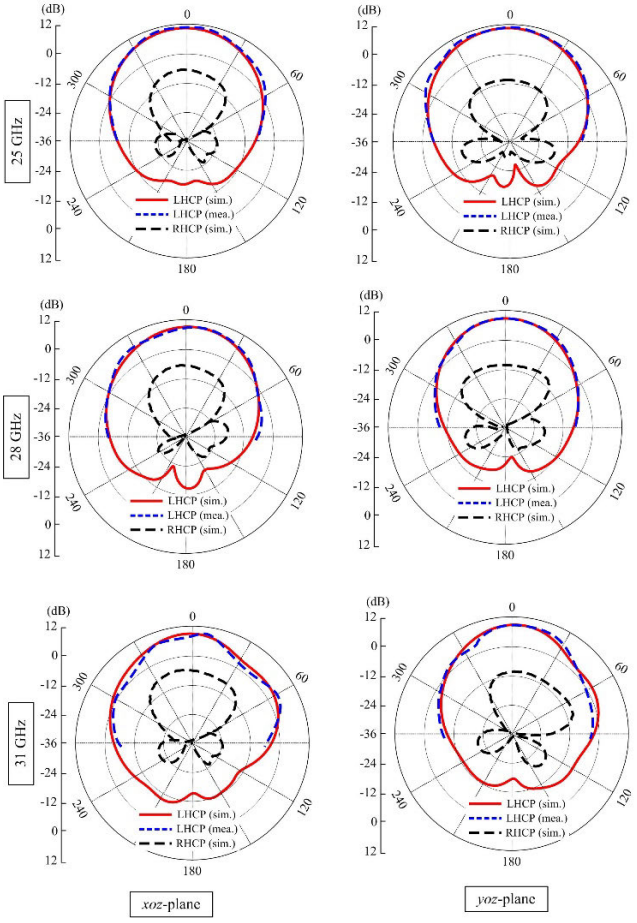

FIGURE 13. Radiation patterns of the proposed metasurface antenna for different frequencies.

at 26 GHz and 28 GHz for various values of $\omega_t(\omega_t = 0°$, $\omega_t = 90°$, and $\omega_t = 180°)$, observed from $+z$-direction is shown in Fig. 14. The E-field rotates in a clockwise direction

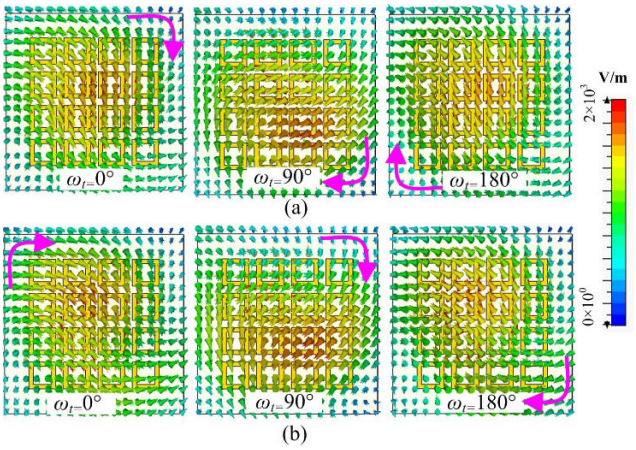

FIGURE 14. Clockwise rotation of the *E*-field, suggesting the LHCP radiations of the proposed antenna.

at both frequencies suggesting the LHCP radiation of the proposed antenna.

D. COMPARISION WITH STATE-OF-THE-ART-WORKS

The performance comparison in terms of overall size, bandwidth, gain, and design simplicity (number of the printed layers and presence of air gap) of the proposed MTS antenna with the state-of-the-art designs is summarized and provided in Table 2. In general, it can be concluded that the proposed antenna has the simplest design and low profile with minimum printed layers having no air gap while possessing wider ($|S_{11}|$ and AR) bandwidths and a moderate gain of 11 dBic. Fabry-Perot antennas [8] have the advantages of high gain but have limited AR bandwidth as well as the design complexity due to multiple printed layers and the air gap. Similarly, stacked patch antennas [9], [14] can produce wide operating bandwidths, suffer from the low gain and

complicated design (multiple printed layers and air gap). Among MTS antennas [16], [17], [28], [29], [33], the designs presented in [17], [28], [29] offer wide bandwidths due to the design freedom at microwave frequencies. Although, these designs have disadvantages of low gain. Meanwhile, the MTS antennas [16], [33] at 5G MWM frequency band, only [16] has CP radiations, however, it possesses three printed layers with an air gap, while the AR bandwidth is restricted to only 6%. Though, the electromagnetic bandgap (EBG) antenna presented in [34] offers a simple design and a very wide impedance bandwidth covering the entire 5G MMW band, has linearly polarized radiation. It is worth mentioning that, among all MWM CP antennas [8], [16], [35]–[39], only the proposed design covers the frequency band (24.2 – 29.5 GHz) adopted globally for 5G communication systems.

VI. CONCLUSION

A low-profile wideband CP patch antenna with high performance using a square ring MTS is presented in this paper. The operating bandwidth of the patch antenna is improved using resonances of truncated corner patch and diagonally slotted patch. Moreover, for the wideband operation to cover the 5G MMW band, a lattice of a periodic layer of square ring MTS is used. The antenna prototype is fabricated and measured to validate the simulated data. The antenna exhibits wide bandwidth from 24 to 34.1 GHz for $|S_{11}| < -10$ with an overlapping AR bandwidth of 20.1 % (24.1 – 29.5 GHz). Additionally, stable radiation patterns with a little gain variation from 9.5 – 11 dBic are also achieved across the operating band. With the aforementioned advantages including low-profile of the antenna ($1.1\lambda_0 \times 1.1\lambda_0 \times 0.093\lambda_0$), the proposed antenna can be a good candidate for 5G MMW systems including smart devices and sensors.

REFERENCES

[1] M. Masoudi, "Green mobile networks for 5G and beyond," *IEEE Access*, vol. 7, pp. 107270–107299, 2019.
[2] R. Vannithamby and S. Talwar, *Towards 5G: Applications, Requirements and Candidate Technologies*. Hoboken, NJ, USA: Wiley, 2017.
[3] J. F. Harvey, M. B. Steer, and T. S. Rappaport, "Exploiting high millimeter wave bands for military communications, applications, and design," *IEEE Access*, vol. 7, pp. 52350–52359, 2019.
[4] Qualcomm Technologies. (Dec. 2017). *Spectrum for 4G and 5G*. Accessed: Aug. 10, 2019. [Online]. Available: https://www.qualcomm.com/news/media-center
[5] N. Hussain, M.-J. Jeong, J. Park, and N. Kim, "A broadband circularly polarized Fabr–Perot resonant antenna using a single-layered PRS for 5G MIMO applications," *IEEE Access*, vol. 7, pp. 42897–42907, 2019.
[6] Z.-G. Liu and W.-B. Lu, "Low-profile design of broadband high gain circularly polarized Fabry–Perot resonator antenna and its array with linearly polarized feed," *IEEE Access*, vol. 5, pp. 7164–7172, 2017.
[7] N. Nguyen-Trong, H. H. Tran, T. K. Nguyen, and A. M. Abbosh, "A compact wideband circular polarized Fabry–Perot antenna using resonance structure of thin dielectric slabs," *IEEE Access*, vol. 6, pp. 56333–56339, 2018.
[8] M. Asaadi, I. Afifi, and A.-R. Sebak, "High gain and wideband high dense dielectric patch antenna using FSS superstrate for millimeter-wave applications," *IEEE Access*, vol. 6, pp. 38243–38250, 2018.
[9] Q. W. Lin, H. Wong, X. Y. Zhang, and H. W. Lai, "Printed meandering probe-fed circularly polarized patch antenna with wide bandwidth," *IEEE Antennas Wireless Propag. Lett.*, vol. 13, pp. 654–657, 2014.
[10] H. Wong, Q. W. Lin, H. W. Lai, and X. Y. Zhang, "Substrate integrated meandering probe-fed patch antennas for wideband wireless devices," *IEEE Trans. Compon., Packag., Manuf. Technol.*, vol. 5, no. 3, pp. 381–388, Mar. 2015.
[11] J. A. Sheersha, N. Nasimuddin, and A. Alphones, "A high gain wideband circularly polarized antenna with asymmetric metasurface," *Int. J. RF Microw. Comput.-Aided Eng.*, vol. 29, no. 7, Jul. 2019, Art. no. e21740.
[12] P. K. T. Rajanna, K. Rudramuni, and K. Kandasamy, "A wideband circularly polarized slot antenna backed by a frequency selective surface," *J. Electromagn. Eng. Sci.*, vol. 19, no. 3, pp. 166–171, Jul. 2019.
[13] Y. Liu, K. Song, Y. Qi, S. Gu, and X. Zhao, "Investigation of circularly polarized patch antenna with chiral metamaterial," *IEEE Antennas Wireless Propag. Lett.*, vol. 12, pp. 1359–1362, 2013.
[14] W. Yang, J. Zhou, Z. Yu, and L. Li, "Single-fed low profile broadband circularly polarized stacked patch antenna," *IEEE Trans. Antennas Propag.*, vol. 62, no. 10, pp. 5406–5410, Oct. 2014.
[15] M. J. Jeong, N. Hussain, J. W. Park, S. G. Park, S. Y. Rhee, and N. Kim, "Millimeter-wave microstrip patch antenna using vertically coupled split ring metaplate for gain enhancement," *Microw. Opt. Technol. Lett.*, vol. 61, no. 10, pp. 2360–2365, Oct. 2019.
[16] M. Akbari, H. A. Ghalyon, M. Farahani, A.-R. Sebak, and T. A. Denidni, "Spatially decoupling of CP antennas based on FSS for 30-GHz MIMO systems," *IEEE Access*, vol. 5, pp. 6527–6537, 2017.
[17] K. Agarwal, Nasimuddin, and A. Alphones, "Wideband circularly polarized AMC reflector backed aperture antenna," *IEEE Trans. Antennas Propag.*, vol. 61, no. 3, pp. 1456–1461, Mar. 2013.
[18] X. Li, J. Yang, Y. Feng, M. Yang, and M. Huang, "Compact and broadband antenna based on a step-shaped metasurface," *Opt. Express*, vol. 25, no. 16, p. 19023, Aug. 2017.
[19] S. X. Ta and I. Park, "Artificial magnetic conductor-based circularly polarized crossed-dipole antennas: 2. AMC structure without grounding pins," *Radio Sci.*, vol. 52, no. 5, pp. 642–652, May 2017.
[20] J. Hu, G. Q. Luo, and Z.-C. Hao, "A wideband quad-polarization reconfigurable metasurface antenna," *IEEE Access*, vol. 6, pp. 6130–6137, 2018.
[21] N. Nasimuddin, Z. N. Chen, and X. Qing, "Bandwidth enhancement of a single-feed circularly polarized antenna using a metasurface: Metamaterial-based wideband CP rectangular microstrip antenna.," *IEEE Antennas Propag. Mag.*, vol. 58, no. 2, pp. 39–46, Apr. 2016.
[22] Q. Chen and H. Zhang, "Dual-patch polarization conversion metasurface-based wideband circular polarization slot antenna," *IEEE Access*, vol. 6, pp. 74772–74777, 2018.
[23] N. Hussain, K. E. Kedze, and I. Park, "Performance of a planar leaky-wave slit antenna for different values of substrate thickness," *J. Electromagn. Eng. Sci.*, vol. 17, no. 4, pp. 202–207, Oct. 2017.
[24] Z. Wu, H. Liu, and L. Li, "Metasurface-inspired low profile polarization reconfigurable antenna with simple DC controlling circuit," *IEEE Access*, vol. 7, pp. 45073–45079, 2019.
[25] N. Hussain and I. Park, "Performance of multiple-feed metasurface antennas with different numbers of patch cells and different substrate thicknesses," *Appl. Comput. Electromagn. Soc. J.*, vol. 33, no. 1, pp. 49–55, 2018.
[26] S. Nelaturi and N. V. S. N. Sarma, "A compact microstrip patch antenna based on metamaterials for Wi-Fi and WiMAX applications," *J. Electromagn. Eng. Sci.*, vol. 18, no. 3, pp. 182–187, Jul. 2018.
[27] J. Park, M. Jeong, N. Hussain, S. Rhee, S. Park, and N. Kim, "A low-profile high-gain filtering antenna for fifth generation systems based on nonuniform metasurface," *Microw. Opt. Technol. Lett.*, vol. 61, no. 11, pp. 2513–2519, Nov. 2019.
[28] C. Zhao and C.-F. Wang, "Characteristic mode design of wide band circularly polarized patch antenna consisting of H-shaped unit cells," *IEEE Access*, vol. 6, pp. 25292–25299, 2018.
[29] L.-M. Si, W. Zhu, and H.-J. Sun, "A compact, planar, and CPW-fed metamaterial-inspired dual-band antenna," *IEEE Antennas Wireless Propag. Lett.*, vol. 12, pp. 305–308, 2013.
[30] T. Li and Z. N. Chen, "Design of dual-band metasurface antenna array using characteristic mode analysis (CMA) for 5G millimeter-wave applications," in *Proc. IEEE-APS Top. Conf. Antennas Propag. Wireless Commun. (APWC)*, Cartagena des Indias, Colombia, Sep. 2018, pp. 721–724.
[31] T. Li and Z. N. Chen, "Wideband substrate-integrated waveguide-fed end-fire metasurface antenna array," *IEEE Trans. Antennas Propag.*, vol. 66, no. 12, pp. 7032–7040, Dec. 2018.
[32] T. Li and Z. N. Chen, "Metasurface-based shared-aperture 5G *S*-/ *K*-band antenna using characteristic mode analysis," *IEEE Trans. Antennas Propag.*, vol. 66, no. 12, pp. 6742–6750, Dec. 2018.

[33] T. Li and Z. N. Chen, "A dual-band metasurface antenna using characteristic mode analysis," *IEEE Trans. Antennas Propag.*, vol. 66, no. 10, pp. 5620–5624, Oct. 2018.
[34] X. Lin, B.-C. Seet, F. Joseph, and E. Li, "Flexible fractal electromagnetic bandgap for millimeter-wave wearable antennas," *IEEE Antennas Wireless Propag. Lett.*, vol. 17, no. 7, pp. 1281–1285, Jul. 2018.
[35] M.-C. Tang, T. Shi, and R. W. Ziolkowski, "A study of 28 GHz, planar, multilayered, electrically small, broadside radiating, huygens source antennas," *IEEE Trans. Antennas Propag.*, vol. 65, no. 12, pp. 6345–6354, Dec. 2017.
[36] W. Lin, R. W. Ziolkowski, and T. C. Baum, "28 GHz compact omnidirectional circularly polarized antenna for device-to-device communications in the future 5G systems," *IEEE Trans. Antennas Propag.*, vol. 65, no. 12, pp. 6904–6914, Dec. 2017.
[37] A. Dadgarpour, M. S. Sorkherizi, and A. A. Kishk, "High-efficient circularly polarized magnetoelectric dipole antenna for 5G applications using dual-polarized split-ring resonator lens," *IEEE Trans. Antennas Propag.*, vol. 65, no. 8, pp. 4263–4267, Aug. 2017.
[38] M. Mantash and T. A. Denidni, "CP antenna array with switching-beam capability using electromagnetic periodic structures for 5G applications," *IEEE Access*, vol. 7, pp. 26192–26199, 2019.
[39] D. M. Elsheakh and M. F. Iskander, "Circularly polarized triband printed quasi-Yagi antenna for millimeter-wave applications," *Int. J. Antennas Propag.*, vol. 2015, Feb. 2015, Art. no. 329453.
[40] J. R. James and P. S. Hall, *Handbook of Microstrip Antennas*. London, U.K.: Peter Peregrinus, 1989.
[41] Nasimuddin, Z. N. Chen, and X. Qing, "Slotted microstrip antennas for circular polarization with compact size," *IEEE Antennas Propag. Mag.*, vol. 55, no. 2, pp. 124–137, Apr. 2013.
[42] K. F. Tong and T. P. Wong, "Circularly polarized U-slot antenna," *IEEE Trans. Antennas Propag.*, vol. 55, no. 8, pp. 2382–2385, Aug. 2007.
[43] K. Lau and K. Luk, "A novel wide-band circularly polarized patch antenna based on L-probe and aperture-coupling techniques," *IEEE Trans. Antennas Propag.*, vol. 53, no. 1, pp. 577–582, Jan. 2005.
[44] K.-F. Tong and J. Huang, "New proximity coupled feeding method for reconfigurable circularly polarized microstrip ring antennas," *IEEE Trans. Antennas Propag.*, vol. 56, no. 7, pp. 1860–1866, Jul. 2008.
[45] F. Costa, O. Luukkonen, C. R. Simovski, A. Monorchio, S. A. Tretyakov, and P. M. De Maagt, "TE surface wave resonances on high-impedance surface based antennas: Analysis and modeling," *IEEE Trans. Antennas Propag.*, vol. 59, no. 10, pp. 3588–3596, Oct. 2011.
[46] D. Ferreira, R. F. S. Caldeirinha, I. Cuinas, and T. R. Fernandes, "Square loop and slot frequency selective surfaces study for equivalent circuit model optimization," *IEEE Trans. Antennas Propag.*, vol. 63, no. 9, pp. 3947–3955, Sep. 2015.

NIAMAT HUSSAIN received the B.S. degree in electronics engineering from the Dawood University of Engineering and Technology, Karachi, Pakistan, in 2014, and the M.S. degree in electrical and computer engineering from Ajou University, Suwon, South Korea. He is currently pursuing the Ph.D. degree in information and communication engineering with Chungbuk National University, Chungju, Korea. His research is mainly focused on lens-coupled antennas, metasurface antennas, metamaterial antennas, UWB antennas, mmWave antennas, and terahertz antennas. He was bestowed with Best Paper Award on 2017, for his presented paper at Korea Winter Conference.

MIN-JOO JEONG received the B.S. degree in electronics engineering from Chosun University, in 2013, and the M.S. degree in LED fusion engineering from Pukyong National University, South Korea, in 2015. He is currently pursuing the Ph.D. degree in information and communication engineering with Chungbuk National University, Chungju, South Korea. His research interests include EMC, antenna design, and EMF.

ANEES ABBAS received the bachelor's degree in telecommunication engineering from BUTEMS, Queta, Pakistan, in 2014. He is currently pursuing the master's degree with the Department of Information and Communication Engineering, Chungbuk National University, South Korea. His research interests include antenna design for WIFI and mobile communication.

TAE-JUN KIM received the bachelor's degree in electrical and electronics engineering from Yonsei University, South Korea, in February 2003, and the Ph.D. degree in electrical engineering from KAIST, Daejeon, South Korea, in February 2011. He worked as a Senior Researcher with the Mobile Media Application Technology Team, ETRI, from October 2011 to August 2013. He is currently an Associate Professor with the School of Information and Communication Engineering, Chungbuk National University, Cheongju, South Korea. His research interest is mainly focused on network systems.

NAM KIM received the B.S., M.S., and Ph.D. degrees in electronics engineering from Yonsei University, Seoul, South Korea, in 1981, 1983, and 1988, respectively. He has been a Professor with the School of Information and Communication Engineering, Chungbuk National University, Chengju, South Korea, since 1989. His scientific interests are focused on optical information processing, the health effect of the EMF, wireless power transfer, and antennas for mobile communications. He is a member of the International Advisory Committee for the World Health Organization project on EMF, the IEEE International Committee on Electromagnetic Safety, and the International Electro Technical Commission TC 106. He was the President of the Bioelectromagnetics Society.